Journal of Photopolymer Science and Technology
Volume 19, Number 2 (2006) 297-304 © 2006 TAPJ

Optical Properties of Rod-like Fluorinated Polyimides and Model Compounds Derived from Diamines having High Electron-donating Properties

Yoshifumi SATO, Masafumi YOSHIDA, and Shinji ANDO*

Department of Organic & Polymeric Materials, Tokyo Institute of Technology, Ookayama 2-12-1-S1-21, Meguro-ku, Tokyo, 152-8552, Japan
e-mail : sando@polymer.titech.ac.jp

The thermal and optical properties of four kinds of aromatic polyimides (PIs) having a common skeletal structure have been investigated using thermogravimetric analysis and UV/Vis absorption and fluorescence spectroscopy. Pyromellitic dianhydride (PMDA) and 1,4-difluoropyromellitic dianhydride (P2FDA) were used as the dianhydrides for model compounds and PIs to examine the charge transfer (CT) nature of the PIs. In addition, methoxy ($-OCH_3$) group was chosen as the side group to introduce strong electron-donating property to the diamines. The PIs derived from P2FDA exhibit an intense and characteristic absorption band at ~550 nm and two independent pairs of the excitation and emission peaks. The spectral data from the model compounds demonstrate that the characteristic absorption/emission at 550 nm is attributable to the local $\pi-\pi^*$ transition within the P2FDA moiety. In contrast, the emissions appearing at the longer wavelengths for the P2FDA-based PIs (720-730 nm) and those for the PMDA-based PIs (540 and 620 nm) are closely related to the charge transfer (CT) interactions between the dianhydride and diamine moieties, and their behaviors accord with the calculated molecular orbital energies using the density functional theory.

Keywords / aromatic polyimide / optical properties / charge transfer / absorption / refractive index / fluorescence / excitation & emission / density functional theory

1. Introduction

The charge transfer (CT) nature of the aromatic PIs was firstly discussed by Dine-Hart et al. [1], and the studies followed by a number of researchers have been clarifying that the CT interactions have significant influences on the electronic and optical properties of PIs, though the thermal properties such as glass transition temperatures can be explained by the chain flexibility.[2] However, the insolubility of the conventional PIs in organic solvents makes difficult to distinguish the influences of intra- and intermolecular interactions. The investigations using organo-soluble model compounds are effective for selective observation of the intra-molecular interactions. Viallat et al.[3] have measured the absorption and fluorescence spectra of solutions of poly(ether imide) (PEI) and its corresponding models and reported that the fluorescence of PEI in the solid state is closely related to the intermolecular packing and the CT nature. Hasegawa and coworkers [4] have observed the absorption and fluorescence spectra for several types of model compounds in order to clarify the photophysical processes in aromatic PIs. They reported that the CT fluorescence observed for the models is mainly originated from the excited intramolecular CT state. Their findings are important to understand the complicated excitation/emission mechanisms in the aromatic PIs.

On the other hand, fluorinated PIs (FPIs) have been attracting much attention as a new class of electronic and optical material due to their thermal stability, good mechanical strength, high transparency, and low refractive indices [5,6]. St.Clair and coworkers have synthesized a series of FPIs containing $-C(CF_3)_2-$ linkages using 4,4'-(hexafluoroisopropylidene)diphthalic dianhydride (6FDA). The FPIs exhibit low dielectric constants, low water absorption, and good environmental

Received April 11, 2006
Accepted May 25, 2006

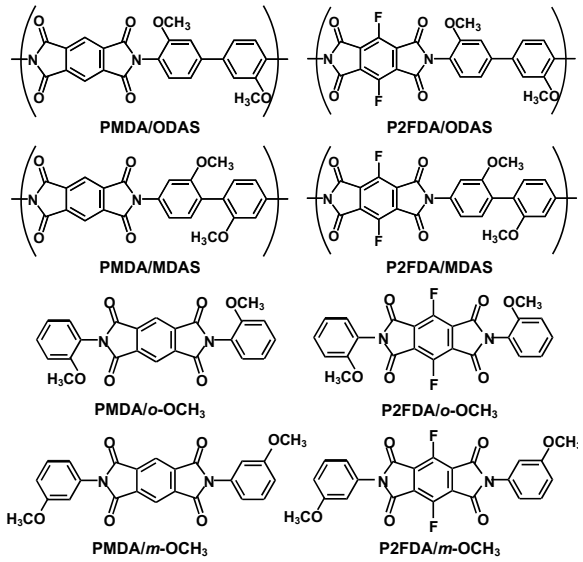

Scheme 1. Structures of the polyimides (PIs) and the corresponding organo-soluble model compounds.

stability. We have also synthesized a series of FPIs and reported their thermal, mechanical, and optical properties.[7] In particular, we have been trying to control the CT nature of aromatic PIs by carefully choosing combinations of diamines and dianhydrides. By using the absorption edges of PI films as measures of representing the degrees of CT interactions, the CT interactions in the solid FPI films synthesized from CF_3–substituded diamines are significantly reduced, but those in the FPIs derived from the dianhydrides whose benzene rings are substituted by $-CF_3$ or –F are strengthened.[8] These behaviors are well explained in term of the CT nature between the electron-donating diamine and the electron-withdrawing dianhydride moieties.[9]

A number of studies have been reported to design and synthesize transparent and colorless FPIs by introducing $-CF_3$ to the skeletal structures of FPIs. However, no attempts have been made to strengthen the CT interactions in the FPIs. Accordingly, we synthesized novel FPIs and their model compounds from rigid-rod diamines containing highly electron-donating methoxy groups and fluorinated dianhydrides exhibiting high electron withdrawing property. In particular, we prepared two kinds of diamines having the common skeletal structure with different positions of methoxy groups to investigate the influence on the CT nature and the electronic structures of the FPIs. The purpose of this study is to measure and examine the thermal and optical properties of the PIs having strong CT interactions with the aid of measurements on organo-sluble model compounds.

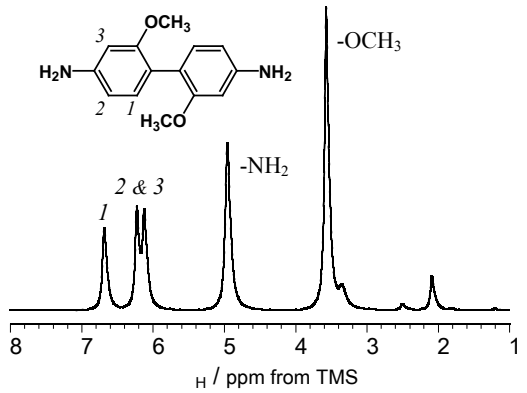

Figure 1. ^{1}H NMR spectrum of 2,2'-dimethoxybenzidine (MDAS) dissolved in $CDCl_3$. This diamine was synthesized through the benzidine rearrangement.

2. Experimental

2.1 Source materials

Pyromellitic dianhydride (PMDA) purchased from Kanto Chemical was purified by sublimation under reduced pressure. 1,4-Difluoropyromellitic dianhydride (P2FDA) supplied by NTT corporation was recrystallized from acetic anhydride/toluene solution and then dried at 110°C for 1h under vacuum. 3,3'-Dimethoxy-4,4'-diaminobiphenyl (ODAS) hydrochloride supplied by Wakayama-Seika was dissolved in distilled water, and then neutralized by aqueous sodium hydroxide. The precipitate was filtered, dried at 50°C for 2h under vacuum, and then purified by sublimation under reduced pressure. 3-Nitroanisole, *ortho*-anisidine (*o*-OCH_3), *meta*-anisidine (*m*-OCH_3), those were purchased from Tokyo Chemical Industry, was used without purification. 2,2'-Dimethoxy-4,4'-diaminophenyl (MDAS) was synthesized according to the literature through the benzidine rearrangement reactions of 3-nitroanisole.[10] The product at each step was identified by ^{1}H- and ^{13}C-NMR using chloroform-*d* ($CDCl_3$) as solvent and FT-IR. The ^{1}H-NMR spectrum of the synthesized MDAS dissolved in $CDCl_3$ is shown in Figure 1 as an example.

2.2 Synthesis of Poly(amic acid)s and Preparation of Polyimide Films

Aromatic PI films were prepared by thermal imidization of their precursors, poly(amic acid)s (PAAs). The molecular structures of aromatic PIs used in this study are shown in Scheme 1. The PAA solutions were prepared by polycondensations of dianhydrides and diamines in *N*,*N*-dimethylacetamide (DMAc). For instance, a PAA solution was prepared by slowly adding the equivalent mole of the sublimed dianhydride to the purified

diamine in dry DMAc in a glove box filled with dry nitrogen (N_2). Once the dianhydride addition was completed, the reaction flask was capped tightly, and stirring was continued for 24–48 h. The polymerization mixture of PAA solutions was completely homogeneous. The solid contents were 10–15 wt % for the precursor solutions. The PAA solutions were spin-coated onto 3-inch silicon substrates, followed by soft-baking at 70°C for 1 h and subsequent thermal imidization in an inert oven with a dry N_2 gas flow by a three-step imidization protocol : 160°C/1 h, 250°C/30 min, and 350°C/ 1 h. The heating rate was 4°C/min.

2.3 Synthesis of Model Compounds

The molecular structures of the model compounds synthesized in this study are also shown in Scheme 1. The amide acid of PMDA/*o*-OCH_3 was synthesized by adding PMDA powder to a DMAc solution of *o*-anisidine (5 mol% excess of PMDA) under N_2, followed by stirring for 12 h at room temperature. *o*-Xylene was added as dehydration agent to the amic acid solution, slowly heated, and kept refluxing at 160°C for 4h for imidization. The precipitate thus obtained was filtered, washed with methanol several times, and then recrystallized from DMAc solution followed by washing by methanol and drying under vacuum at 120°C for 8h. The amide acid of PMDA/*m*-OCH_3 was synthesized in a similar manner.

The amide acid of P2FDA/*o*-OCH_3 was synthesized by adding P2FDA powder to a DMAc solution of *o*-anisidine under N_2, followed by stirring for 12 h at room temperature. Then, the solution was poured into distilled water, and the precipitate was filtered and dried at 160°C for 24 h under vacuum. The solid thus obtained was slowly heated and kept at 200°C for 4h for imidization and then recrystallized from ethylacetate.

The amide acid of P2FDA/*m*-OCH_3 was synthesized by adding P2FDA, *m*-anisidine (5 mol% excess of P2FDA), and sodium acetate (half molar amount of P2FDA) to acetic acid and then refluxed at 120°C for 3h, followed by pouring into excess amount of boiling water. The precipitate was cooled to room temperature, filtered, and washed by boiling water for several times. The powder thus obtained was recrystallized from DMSO/ethanol, followed by refluxing in ethanol to extract the residual DMSO absorbed in the solids. All product at each step was identified by ^{1}H- / ^{13}C-NMR using dimethyl-d_6 sulfoxide (DMSO-d_6) or chloroform-*d* ($CDCl_3$) as solvents and FT-IR.

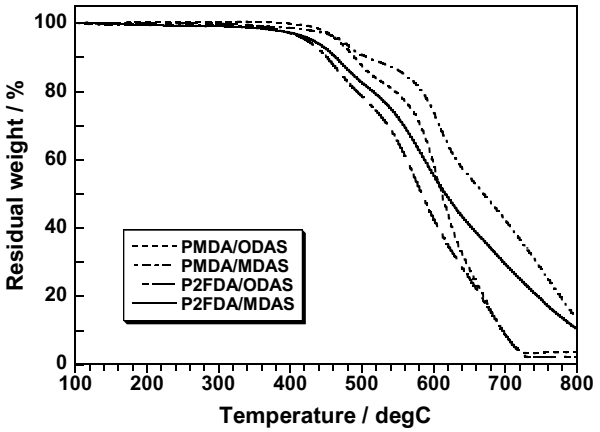

Figure 2. TGA curves of the PIs. Two-step degradation behaviors are observed for all the PIs.

2.4 Measurements

^{1}H- and ^{13}C-NMR spectra were measured with a JEOL GSX-500 spectrometer. ^{1}H- and ^{13}C-chemical shifts were calibrated with the signals of the internal tetramethylsilane (TMS). Fourier transformed infrared (FT-IR) absorption spectra were measured with a ThermoNicolet Avatar-320 spectrometer equipped with a Thunderdome attenuated total reflection (ATR) attachment. UV/visible absorption spectra were measured using a Hitachi U-3500 spectrophotometer, and fluorescnce (excitation and emission) spectra were measured using a Hitachi F-4500 fluorescent photometer using the reflection set-up. The average thicknesses of the PI films used for absorption and fluorescent measurements were ca.4 μm and 1 μm, respectively. The polarization dependent refractive indices of PI films were measured with a Metricon PC-2000 Prism Coupler, in which a laser source radiating in the near-IR (1.31 μm) was used to minimize the influence of anomalous dispersion near the absorption edges. All the optical measurements were conducted at ambient temperature without humidity control. Thermogravimetric analyses (TGA) were conducted with a Shimadzu TG-50 analyzer. The specimen dimension was 5 x 15 mm, and the heating rate was 10°C/min.

2.5 DFT Calculations

The level of theory with the three-parameter Becke-style hybrid functional (B3LYP) was adopted for the density functional theory (DFT) calculations in conjunction with the Pople-type 6-311G(d,p) basis set. The geometry optimization under no constraints and the calculations of molecular orbital (MO) energies were performed using the Gaussian-98 software installed on a Compaq Alpha server GS-320.

3. Results and Discussion

3.1 Thermogravimetric Analysis

Figure 2 shows the TGA curves measured for the four kinds of PI films. The 5 wt% degradation temperatures (T_d^5) are 466°C, 471°C, 423°C, and 432°C for PMDA/ODAS, PMDA/MDAS, P2FDA/ODAS, P2FDA/MDAS PIs, respectively. The lower thermal stability of P2FDA-based PIs can be ascribed to the degradable phenyl(Ph)–F bonds in the P2FDA moiety. In addition, two-step degradation behaviors are observed for all the PIs. At higher temperatures, significant weight losses are observed in the same temperature range (460–520°C), and the weight losses of 18–25 wt% agree well with the degradation of methoxy (-OCH_3) groups. As a result, the Ph–F bonds cleavage occurs for the P2FDA-based PIs in the early stage, but the degradation of -OCH_3 groups subsequently occurs for all the PIs above 460°C. Further, DSC thermograms were measured for the PI films but no glass transition behaviors were observed below the temperatures at which polymer degradations commence. The absence of glass transition can be ascribed to the rigid-rod molecular structures as reported for PMDA/TFDB PI.[7]

3.2 Refractive Indices and Birefringence

Figure 3 show the refractive indices observed for the PI films (~10 μm-thick) formed on Si substrates. The n_{TE} and n_{TM} represent the refractive indices parallel (TE : transverse electric) and perpendicular (TM : transverse magnetic) to the film plane. The in-plane/out-of-plane birefringence (Δn), defined as the difference between n_{TE} and n_{TM}, can be a good measure for the degrees of molecular rigidity and the orientation of PI main chains. All the PI films demonstrate significantly large values of Δn compared with conventional PIs, which reflect the rigid-rod molecular structures and the significant in-plane orientations onto the substrates. Note that the average refractive indices ($\bar{n}$), which

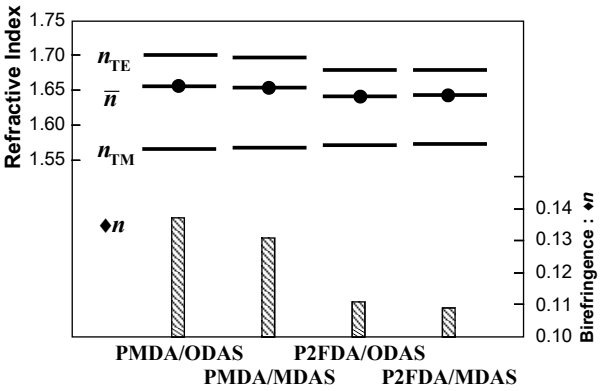

Figure 3. Refractive indices (n) and birefringence (Δn) of the PIs measured at 1310 nm. The n_{TE} and n_{TM} are the refractive indices parallel and perpendicular to the film plane. The Δn is defined as n_{TE}–n_{TM}.

is defined as

$$\bar{n}^2 = \frac{2n_{TE}^2 + n_{TM}^2}{3}$$

and the values of Δn for the PIs derived from P2FDA are smaller than those from PMDA. The decreases in $\bar{n}$ originate from the weakly polarizable fluorines in the P2FDA moiety, and the decrease in Δn is attributable to the reduction of the degrees of molecular packing and in the order of inter-molecular orientations. We have reported that the molecular packing coefficient (K_p), that can be estimated from the observed refractive indices and the calculated molecular polarizability, can be used as a measure for the degree of density of molecular packing of PIs.[11] The estimated values of K_p are 0.612, 0.612, 0.613, and 0.617 for PMDA/ODAS, PMDA/MDAS, P2FDA/ODAS, P2FDA/MDAS PIs, respectively. These values indicate that 1) the diamine structures are not influential to the molecular packing, and 2) the difluorination of PMDA slightly increases the molecular packing, which may be reflected on the optical properties of the PIs.

Table 1. The molecular orbital energies (ε) of HOMO and LUMO (eV), energy gaps (Δε /eV), thermal degradation temepratures of 5wt% (T_d /°C), refractive indices for the TE and TM polarizations, average refractive indices, birefringence, absorption edges (λ_E /nm), excitation and emission peaks (λ_{ex}, λ_{em} /nm) in the fluorescence spectra.

polyimide	ε_{HOMO}	ε_{LUMO}	Δε	T_d^5	n_{TE}	n_{TM}	n	Δn	λ_E	λ_{ex}	λ_{em}
PMDA/ODAS	-5.92	-3.09	2.83	466	1.702	1.565	1.656	0.137	496	478	539
PMDA/MDAS	-5.68	-3.21	2.47	471	1.698	1.567	1.654	0.131	559	567	622
P2FDA/ODAS	-5.97	-3.42	2.55	423	1.680	1.569	1.642	0.111	752	568 / 665	624 / 722
P2FDA/MDAS	-5.74	-3.53	2.21	432	1.680	1.571	1.644	0.109	728	578 / 679	634 / 731

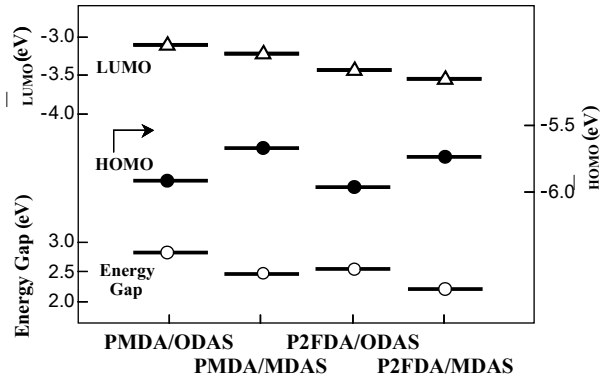

Figure 4. Molecular orbital energies (ε) and energy gaps calculated for the model compounds using DFT. The energy gap is defined as $\varepsilon_{LUMO}-\varepsilon_{HOMO}$.

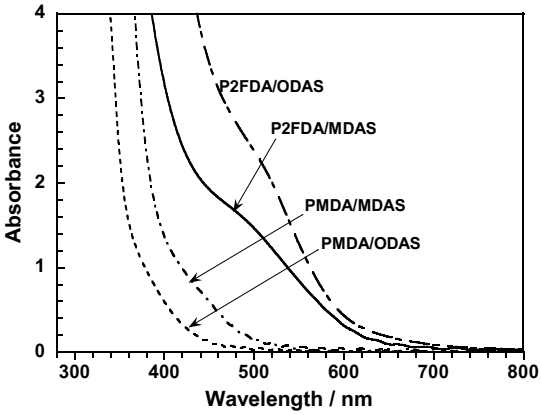

Figure 5. Optical absorption spectra of the PI films (ca.4 μm-thick). The PIs derived from P2FDA exhibit distinct shoulders at around 550 nm.

3.3 Calculation of Molecular Optical Energies

The calculated electron affinity (E_a) of P2FDA (2.48 eV) is significantly higher than that of PMDA (2.13 eV), indicating that the electron-withdrawing property of P2FDA is larger than that of PMDA. In addition, the calculated ionization potential (I_p) of MDAS (6.20 eV) is smaller than that of ODAS (6.34 eV), indicating that the electron-donating property of MDAS is larger than that of ODAS. Figure 4 and Table 1 show the molecular orbital energies (ε) of HOMO and LUMO, and their difference (energy gap) calculated for four kinds of model compounds corresponding to the PIs. P2FDA/MDAS and PMDA/ODAS having the smallest and the largest energy gaps should posses the strongest and the weakest CT interactions, respectively. This trend is essentially consistent with that expected from the combinations of the E_a of dianhydrides and the I_p of diamines. This fact demonstrates that the electronic structures of the source materials remain in the corresponding PIs, and the combinations of the electron-withdrawing P2FDA and the electron-donating MDAS is expected to generate the smallest gap, which should cause the strongest CT.

3.4 Optical Absorption Spectra

Figure 5 shows the UV/Vis absorption spectra for the PIs formed on silica substrates with the thicknesses of ca.4 μm. The absorption edges (λ_E) listed in Table 1 were estimated as the wavelengths at which the values of absorbance reach to 0.05. The PIs exhibit pale-yellow (PMDA-based PIs) to red-dark brown (P2FDA-based PIs) colors. Note that all the source materials used in this study were obtained as colorless (snow white) crystalline powder. However, yellowish colors have appeared during the synthesis of the PAAs from PMDA, and bright reddish colors were observed for those from P2FDA. These characteristic changes in colors are frequently observed in the preparations of PAAs, and they have been discussed in terms of the intra- and inter-molecular CT interactions. The significant bathochromic (long-wavelength) shifts of λ_E observed for PMDA/MDAS than PMDA/ODAS strongly suggest the high CT interactions in the former PI due to the ascending HOMO of MDAS. We have discussed the coloration of aromatic PIs in terms of the CT interactions that can be inferred from the electronic properties of the source materials.[8]

On the other hand, the PI films derived from P2FDA exhibit distinct shoulder peaks around 550 nm and very large λ_Es approaching to 750 nm. Both of the PIs exhibit reddish brown colors. To our best knowledge, such long λ_Es have never been reported for PIs containing no dye-components. It should be pointed out that the characteristic peak observed around 550 nm does not displace depending on the electron-donating properties of diamines (ODAS or MDAS). This fact clearly indicates that the peak is not originated from the inter-molecular CT formation but from the local excitation at the P2FDA moiety including the possibility of intermolecular dimer formation between two or more P2FDA moieties. Since the significant bathochromic shifts of λ_E for the P2FDA-based PIs are primarily determined by the skirts of the characteristic peak, they do not reflect the CT nature of the PIs, and the order of λ_E can not be explained in terms of the CT interactions.

The absorption spectra of the model compounds corresponding the PIs are shown in Figures 6 and 7. The models derived from PMDA are soluble in DMSO but insoluble in acetone. The shoulder peak observed at ca.320 nm for the models can be assigned to the π–π* transitions at the phenyl ring of PMDA moiety [12]. On the other hand, the

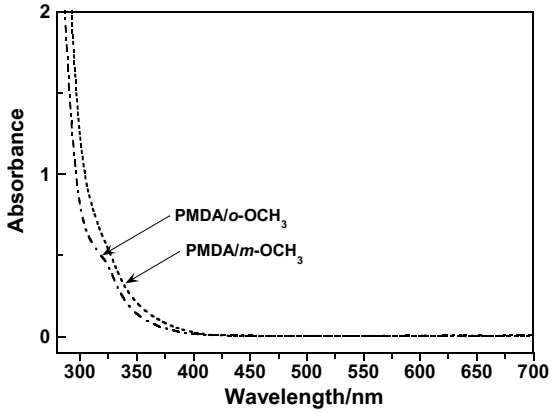

Figure 6. Absorption spectra of the DMSO solutions of the models derived from PMDA (2.0 x 10^{-4} M).

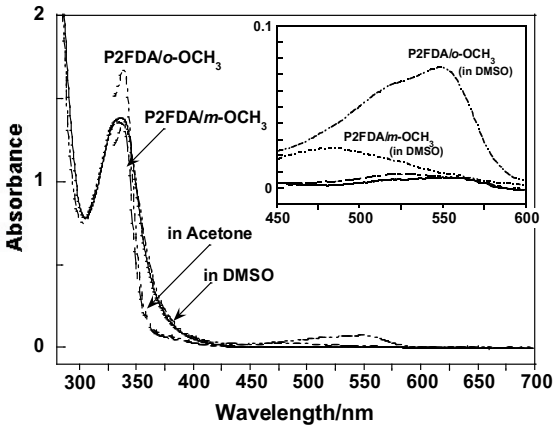

Figure 7. Absorption spectra of the acetone and DMSO solutions of the models derived from P2FDA (2.0 x 10^{-4} M). The intensities of the peak around 550 nm are appreciably intensified in DMSO.

models derived from P2FDA exhibit two absorption peaks at ca.340 nm and ca.550 nm. The former can be assigned to the localized π–π* transitions within the phenyl ring of the P2FDA moiety because these are in the same region as those for the PMDA models, and the peak positions are insensitive to the polarity of solvents. In contrast, the characteristic peaks observed at 550 nm are displaced to longer wavelengths as the polarities of solvents increases (acetone→DMSO). Since *n*–π* transitions should exhibit the opposite displacements, this peak can be tentatively assigned to the π–π* transitions exited from the imide carbonyl (C=O) to the phenyl ring of P2FDA. Figure 8 shows the relationship between the concentration of models (log *c*) and that of the absorbance at 550 nm. The linear relationship in the figure also suggests that this peak is not significantly influenced by the intermolecular CT transitions.

3.5 Fluorescence Excitation/Emission Spectra

Figure 9 show the excitation/emission spectra of the four kinds of PI films (ca.10 μm-thick). The

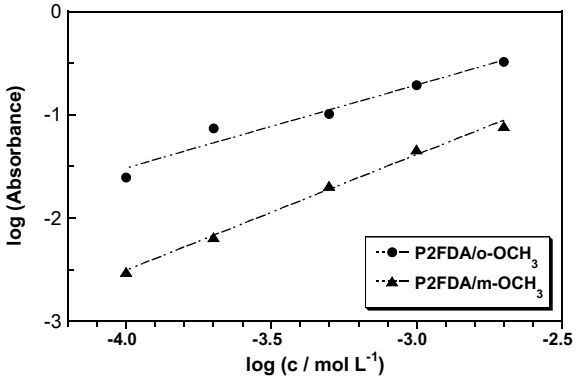

Figure 8. Concentration dependence of the absorptions of the models derived from P2FDA.

order of the excitation/emission peaks is PMDA/ODAS < PMDA/MDAS < P2FDA/ODAS < P2FDA/MDAS from the shorter to longer wavelengths. The excitation/emission peaks for the P2FDA-based PIs are resonated at much longer wavelengths than those for the PMDA-based PIs. Note that the latter PIs show a one-to-one correspondence of the excitation/emission peaks but the former PIs show two pairs of one-to-one correspondence of the excitation/emission peaks. These facts suggest that two independent mechanisms exist in the P2FDA-based PI systems. In particular, the emission peaks for P2FDA/ODAS and P2FDA/MDAS appear at 720–730 nm, when they are excited at 665 nm and 679 nm, respectively. Tang et al. [13] have assigned the weak absorption/emission peaks in aromatic PIs appearing at the longest wavelengths to the intermolecular CT bands because they are shifted to longer wavelengths as the duration at the highest curing temperature increases. Considering the experimental facts that the peaks in the excitation spectra agree well with those of the absorption edges for the PIs, we can also assign the absorption and emission at the longest wavelengths to the intermolecular CT bands. In contrast, the excitation peak appearing at 568 nm for P2FDA/ODAS and that at 578 nm for P2FDA/MDAS agree with the characteristic absorptions at ca.550 nm as shown in Fig. 5. This excitation/emission mechanism can be attributed to the transition between the ground state and the excited intra-molecular CT state.

Figure 10 shows the excitation/emission spectra of the two kinds of models derived from P2FDA, in which the characteristic excitation peak is also observed around 550 nm. This peak shows essentially the same properties as those observed for the PIs derived from P2FDA. This peak displaces to longer wavelengths as the polarities of solvents increases, but the peak positions are insensitive to

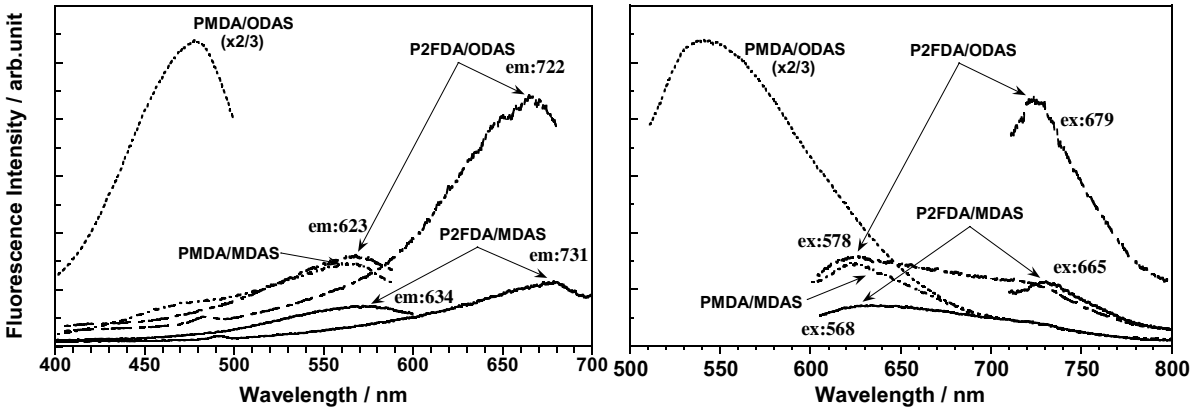

Figure 9. Excitation (left) and emission spectra of the PI films synthesiezed from PMDA and P2FDA. The former PIs show one-to-one correspondence of the excitation/emission peaks, whereas the latter PIs show two pairs of one-to-one correspondence of the excitation/emission peaks.

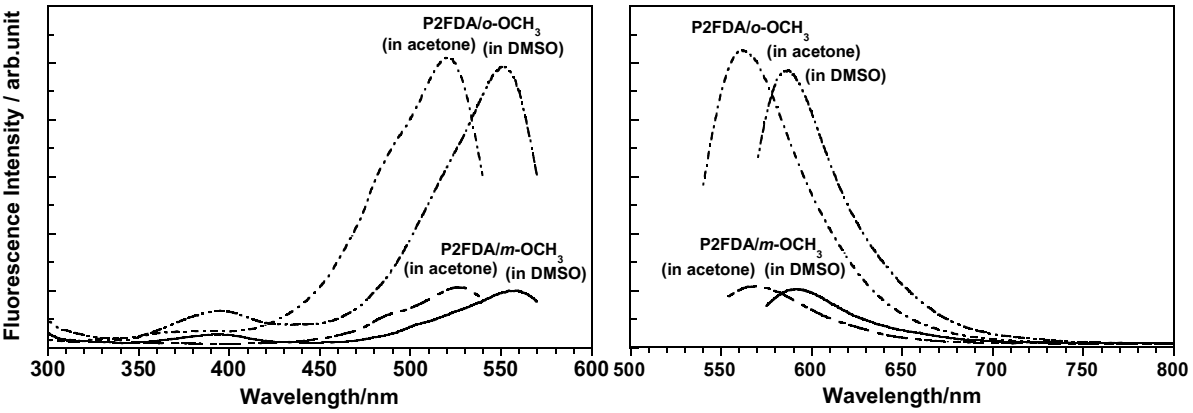

Figure 10. Excitation (left) and emission spectra of the PI films synthesiezed from PMDA and P2FDA. The former PIs show one-to-one correspondence of the excitation/emission peaks, whereas the latter PIs show two pairs of one-to-one correspondence of the excitation/emission peaks.

the diamine structures (with different positions of –OCH_3 groups). Hence, it was assigned to the π–π* transitions excited from the imide carbonyl (C=O) to the phenyl ring within the P2FDA moiety.

In contrast, no fluorescence is observed for the models derived from PMDA. Barashkov et al. [15] have reported that only the phosphorescence was observed for *N*,*N*'-diphenyloxide pyromelliteimide, but no fluorescence was observed. According to the time-dependent (TD)-DFT calculations, the intramolecular electron transition with the lowest energy for the PMDA-based compounds is not π–π* transition but *n*–π* transition from the lone-pair orbital at the carbonyl group to the π* orbital on the phenyl ring of PMDA. Hence, the intersystem-crossing from the singlet $S_{\pi-\pi^*}$ to the triplet $T_{\pi-\pi^*}$ efficiently occurs and emit the phosphorescence.

It should be noted that the excitation/emission peaks observed for the PIs derived from P2FDA are located at longer wavelengths than those from PMDA regardless of the structures of diamines. The bathochromic shifts for the PIs are principally ascribed to the lowering of the LUMO energy due to the fluorines, which may promote and strengthen the CT transitions at the P2FDA moiety.

In addition, the excitation/emission peaks observed for the PIs derived from MDAS are located at longer wavelengths than those from ODAS. Firstly, these shifts can be ascribed to the high electron-donating property of MDAS. Secondly, when the imide bonds are formed between the dianhydrides and ODAS, significant steric hindrance occurs between the imide-plane and the phenyl ring having -OCH_3 group. Therefore, the two aromatic planes cannot be coplanar in the ODAS-based PIs. The DFT calculations demonstrate that the most stable dihedral angles (ω) between the imide-plane and the adjacent phenyl ring are 65° for the ODAS-based PIs but 45° for the MDAS-based PIs. The former conformation should weaken the intra-molecular CT interactions.

As shown in Figure 10, the order of the intensities of CT fluorescence appearing at the

longest wavelengths is PMDA/ODAS > P2FDA/ODAS = PMDA/MDAS > P2FDA/MDAS (in the decreasing order), which represents the degree of CT interactions. This coincides well with the report that an increase in the CT interactions reduces the fluorescence intensity and increase the non-radiative transitions.[14] In addition, the fact that the fluorescence intensity observed for PMDA/ODAS is higher than that of PMDA/MDAS indicates that the more twisted conformation in PMDA/ODAS weaken the CT interactions that cause fluorescence quenching. As a result, the excitation/emission behaviors represented by the peak positions and their fluorescence intensities in the four PIs can be consistently accounted in terms of the degree of CT interactions originated from a) the electron-accepting/donating properties of the source materials (dianhydride and diamines), and b) the stable conformations at the imide bonds.

4. Conclusions

The P2FDA-based PI films exhibit distinct shoulder peaks around 550 nm and very larger values of λ_E of up to 750 nm. The significant bathochromic shifts are primarily originated from the reduced band gaps between the HOMO and LUMO caused by the lowered LUMO energy at the P2FDA moiety. The wavelengths of the characteristic peaks observed at ca.550 nm are insensitive to the diamine structure (the position of $-OCH_3$), which indicates that the peak originates from the local excitation at the P2FDA moiety. Since the same peak observed for the models from P2FDA are displaced to longer wavelengths as the polarities of solvents increases, they can be assigned to the π–π^* transitions from the imide carbonyl group to the phenyl ring of P2FDA.

The excitation/emission peaks are observed for the P2FDA-based PIs at much longer wavelengths (720-730 nm) than those for the PMDA-based PIs (540 and 620 nm). In addition, the former PIs demonstrate two pairs of the excitation/emission peaks but the latter PIs demonstrate simple one-to-one correspondence of the excitation/emission peaks. The characteristic absorption/excitation peaks are observed around 550 nm for the PIs and the models derived from P2FDA. These peaks displace to longer wavelengths as the polarities of solvents increases, but the peak positions are insensitive to the diamine structures. Considering the agreement between the excitation/emission peaks for the PIs and the models, the excitation/emission appearing at the shorter wavelengths can be assigned to the π–π^* transitions within the P2FDA moiety.

In contrast, the excitation peaks for the longer emission peaks observed for the P2FDA-based PIs and the emission peaks for the PMDA-based PIs agree well with the absorption edges. The order of the excitation/emission peaks for the PIs is PMDA/ODAS < PMDA/MDAS < P2FDA/ODAS < P2FDA/MDAS from the shorter to longer wavelengths, which coincides well with the order of the CT interactions that can be predicted from the models.

The excitation/emission peaks observed for the PIs synthesized from ODAS are located at shorter wavelengths than those from MDAS. The strong steric hindrance between the imide-plane and *o*-methoxy group in the ODAS-based PIs and the models significantly weaken the CT interactions. In addition, the inherently weaker electron-donating property of ODAS provides the strong fluorescence appearing at the shorter wavelengths.

References

[1] R. Dine-Hart and W.W. Wright, *Macromol.Chem.*, **143**, 189 (1971).

[2] D. J. Lee, *JMS, Rev. Macromol., Chem. Phys.*, **C29**, 431 (1989).

[3] A. Viallat, R.P. Bom, and J.P. Cohen, *Polymer.*, **35**, 13 (1994).

[4] M. Hasegawa, Y, Shindo, T. Sugimura, S. Ohshima, K. Horie, M. Kochi, R. Yokota, and I. Mita, *J. Polym. Sci. Part B* , **31**, 1617 (1993).

[5] H. Reuter, H. Franke, and C. Feger, *Apple. Opt.*, **27**, 4565 (1988).

[6] A.K. St.Clair, T.L. St.Clair, and K.I.L. Shevket, *Polym. Mat. Sci. Eng.*, **51**, 62 (1984).

[7] S. Ando, *J. Photopolym. Sci. Technol.*, **17**(2), 219-232 (2004). S. Ando, T. Matsuura, and S. Sasaki, Chaps.14 and 15 in "*Fluoropolymers 2 : Properties"*, Eds. G. Hougham et al., Kluwer Academic/Plenum Publishers New York (1999).

[8] S. Ando, T. Matsuura, and S. Sasaki, *Polym. J.*, **29**, 69 (1997).

[9] S. Ando, T. Matsuura, and S. Sasaki, *J. Polym. Sci, Part A, Polym. Chem.*, **30**, 2285 (1991).

[10] S.M. Pyo, S.I. Kim, T.J. Shin, Y.H. Park, and M. Ree, *J. Polym. Sci. Part A, Polym.Chem.,* **37**, 937 (1999).

[11] Y. Terui and S. Ando, *J. Polym. Sci. Part B: Polym. Phys.*, **42**, 2354 (2004).

[12] H. Ishida, S.T. Wellinghoff, E. Baer, and J.L. Koenig, *Macromolecules.*, **13**, 840 (1980).

[13] H. Tang, H. Feng, H. Luo, H. Dong, and Z. Feng; *Eur. Polym. J.*, **33**, 519 (1997).

[14] M. Hasegawa, J. Ishii, and Y. Shindo, *J. Polym. Sci., Part B, Polym. Phys.*, **36**, 827 (1998).

[15] N.N.Barashkov, L.I.Semenova and R.N. Nurmukhametov, *Polym.Sci.USSR.*, **25**, 1264 (1983).